



Effect of calendering on paper surface micro-structure: A multi-scale analysis

Pierre Vernhes*, Jean-François Bloch, Anne Blayo, Bernard Pineaux

EFPG, 461 rue de la papeterie, BP 65, 38402 Saint-Martin d'Hères, France

ARTICLE INFO

Article history:

Received 29 October 2008

Received in revised form 26 January 2009

Accepted 12 March 2009

Keywords:

Surface

Micro-structure

Topography

Surface modification

ABSTRACT

Paper is a complex composite material. Its structure and surface greatly influence its end use properties. Calendering is a finishing process applied to paper to provide a shiny surface and to improve the smoothness. Hence, the control of the efficiency of calendering and the characterization of the final product necessitate the measure of the surface modification. Furthermore the relationship between the surface and the obtained level of gloss has to be further developed. The main purpose of this study is to describe the modification of the micro-structure at various scales of the paper surface due to the calendering process (under various processing conditions). The characterization of the paper surface was carried out thanks to an optical device allowing the topographic measurement to be taken at various scales. The equipment combines topographical imaging with a high definition camera, allowing measurement on the exact same area of the sample after each pass in the nip. We therefore introduce a new way to perform multi-scale analysis of the paper surface modification based on fractal theory.

© 2009 Elsevier B.V. All rights reserved.

1. Introduction

Paper is a complex composite material. Its structure and surface greatly influence its runnability and its printability. Chinga and Helle (2002) studied the influence of the surface topography of both paper and coated paper on the printability using image analysis. The paper structure was characterized by Roscoat et al. (2007) and Bloch et al. (2006) using synchrotron X-ray microtomography. They have demonstrated the sensitivity of the three-dimensional fiber networks to the environmental condition (humidity and temperature) and investigated the relationship between printability and 3D structure. The correlation between the paper ink interaction and the surface and the substrate was investigated by Vernhes et al. (2008b). There exist different processes to provide a shiny surface and to improve the smoothness. Calendering is a finishing process applied to paper. During calendering paper is passed between several pairs of heated rollers. This operation therefore consists of a thermo-mechanical treatment of the paper surface. The calendering process can be performed using either a single nip (Hamel and Dostie, 1997), or multi-nip passes (Holmstad et al., 2004). Hence, the control of the efficiency of the calendering process and the characterization of the final product necessitate the measuring of the surface modification (Table 1).

The paper surface and structural transformations occurring in the nip of the calendering are mostly permanent. The thickness of the sheet decreases and the gloss increases (Litvinov and Farnood, 2006) as a result of the compaction. According to Lepoutre and Means (1978) heat influences the micro-roughness while the pressure influences the macro-roughness. Successful calendering therefore depends on a balance between achieving the best possible surface properties without impairing too many other paper properties (Suontausta, 2002).

The paper surface characterization is also crucial for understanding light reflection that controls the level of gloss. Beland and Bennet (2000) related the micro-facets structure of the surface to the gloss. Different approaches of surface characterization were carried out: Chinga (2004) used laser profilometry and electronic microscopy, Arney et al. (2006) developed a specific optical device dedicated to paper surface analysis. Gloss is strongly dependent on the surface roughness; a high roughness leads to low gloss (Gate et al., 1973). Alexandra-Katz and Barrera (1998) emphasises two key parameters to relate surface topography and gloss level: the root mean square (S_q) and the correlation length (L_c). Like other materials, the value of paper roughness is strongly dependant on the evaluation length (Bigerelle et al., 2007) and on the discretization step (Wu, 2000). However the influence of these two factors was not systematically taken into account to characterize paper surface. Indeed, small scale measurements are often associated with optical properties of paper such as gloss while large scale measurements (Lettieri et al., 1993) are dedicated to the characterization of surface homogeneity and machinability (Patrikar, 2004). Therefore, multi-scale analysis is needed to separate the contribution of the different roughness sizes.

* Corresponding author.

E-mail addresses: Pierre.vernhes@efpg.inpg.fr (P. Vernhes), Jean-francois.bloch@efpg.inpg.fr (J.-F. Bloch), Anne.blayo@efpg.inpg.fr (A. Blayo), Bernard.pineaux@efpg.inpg.fr (B. Pineaux).

Table 1
Calendering condition.

Code	Pressure (bar)	Hard roll temperature (°C)	Numbers of nips
C1	40	100	1–6
C2	40	20	1–6
C3	25	100	1–6
C4	25	20	1–6

The main purpose of this study is to describe the modification to the micro-structure of the paper surface due to the calendering process. Different processing conditions were used here. The characterization of the paper surface was carried out thanks to an optical device allowing the topographic measurement to be taken at various scales. The equipment combines topographical imaging with a high definition camera allowing measurement on the exact same area after each pass in the nip. Multi-scale analyses were performed to characterize the effect of calendering on the paper surface. The influence of both temperature and pressure on the evolution of S_q and L_c was studied on two different papers using a fractal approach.

2. Materials and methods

2.1. Physical paper properties of the chosen samples

We chose two types of office paper referenced to as Q+ (basis weight 81 g m⁻² and thickness 120 μm) and Q- (basis weight 110 g m⁻² and thickness 124 μm), respectively. These types of paper are common office paper: Q+ is assumed to have a better quality than Q-.

2.2. Description of the topographic equipment

We used the Infinite Focus Measurement Machine® (IFM) which is an optical measurement device. It allows for the acquisition of dataset at high depth of focus similar to the Scanning Electron Microscopy.

The main component of this optical metrology instrument is a precision optic consisting of various lens systems. It can be equipped with different objectives allowing measurements with different resolutions. With a beam splitting mirror, light emerging from a white light source is inserted into the optical path of the system and focused onto the specimen via the objective. Depending on the topography of the specimen, the light is reflected into several directions as soon as it hits the specimen. All rays emerging from the specimen and hitting the objective are bundled in the optics and gathered by a light sensitive sensor behind the beam splitting mirror. Due to the small depth of field of the optics only small regions of the object are sharply imaged. To allow a complete detection of the surface with full depth of field, the precision optic is moved vertically along the optical axis. A sensor captures a series of 2D datasets during this scanning process. All sensor parameters are optimized at each vertical position according to the reflective properties of the surface. After the scanning process, the 2D datasets are evaluated to generate 3D information. This is achieved by analyzing the variation of focus along the vertical axis. Once all height measurements are determined, an image with full depth of field is computed. An important characteristic of the system is that it not only delivers topographical information but also an optical colour image of the surface. The technology on which the system is based has recently been included into ISO standards (ISO 25178-6, 2007) classifying different methods for surface texture extraction. Five different objectives were used: 5×, 10×, 20×, 50× and 100× giving a lateral resolution of 1.6 μm, 800 nm, 400 nm, 160 nm and 80 nm, respectively. For the 100× and 50× magnification, the sampling distance is shorter than the light wavelength. Hence the “real” lateral

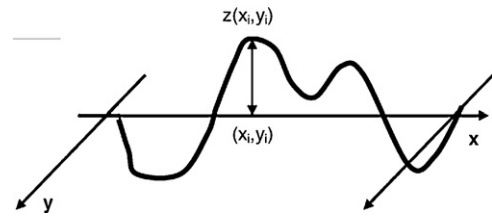


Fig. 1. Schematic description of the calculation of the parameter S_q from the surface mapping $z(x, y)$.

resolution is then limited by the light wavelength and specified to be 400 nm. However, the apparent resolution is 160 nm and 80 nm. The image resolution is 1024 × 1280 pixels.

Parameters are calculated according to the mean plan. No data treatment is carried out; the raw data are only treated in order to compare the different scales of measurements. Samples were installed on a stage to ensure a good flatness.

2.3. Statistical parameters

A large number of statistical parameters exist aiming to describe surface features. We mainly focused on two of them: S_q describes the amplitude of the surface and L_c describes the lateral feature of the surface. The roughness parameters are evaluated for an $M \times N$ rectangular sampling area with the lateral directions x and y and vertical direction z . Statistical parameters are calculated from the raw data according to the mean plan departure of the measured surface.

S_q is a dispersion parameter defined as the root mean square value of the surface departures within the sampling area. The RMS deviation of surface topography (S_q) is defined as

$$S_q = \sqrt{\frac{1}{MN} \sum_{j=1}^N \sum_{i=1}^M z(x_i, x_j)^2} \tag{1}$$

Fig. 1 shows how the calculation is carried out from the measurement data.

Statistical roughness parameters including the various moments of the height distribution (like S_q) are related to the single-point correlation of surface heights, whereas Fourier methods such as Areal Autocorrelation Function (ACCF) are based on a two-point correlation, which characterizes the correlation heights at two different positions (Stout, 2000). For three-dimensional surface topography, the ACCF may be considered from an areal topographic point of view:

$$ACCF(\Delta x, \Delta y) = \sum_{k=0}^{M-1-\Delta xN-1-\Delta y} \sum_{t=0}^{N-1-\Delta xN-1-\Delta y} z(x_k, y_t)z(x_{k+\Delta x}, y_{t+\Delta y}) \tag{2}$$

where Δx and Δy are the difference in position between two height values in lateral directions, respectively.

The autocorrelation function for a surface profile is calculated by sequentially stepping the profile across a stationary copy, multiplying, and normalizing (see Eq. (2)). This function is unity for 0 steps, or lags, and drops as the number of lags increases.

The rate of the drop-off, measured by the shortest lag at which the autocorrelation value equals $1/e$, is called the correlation length, L_c (the mathematical expression is given by Eq. (3)):

$$L_c = \text{MIN} \sqrt{\Delta x^2 + \Delta y^2} \quad \text{with} \quad ACCF(\Delta x, \Delta y) \leq 1/e \approx 0.37 \tag{3}$$

Fig. 2 summarizes the calculation and the physical meaning of L_c calculated from both surface and profile.

Smoother surfaces have larger correlation lengths. Both S_q and L_c values depend on the step of discretization (which is the length between two consecutive points) and the surface size of the sample.

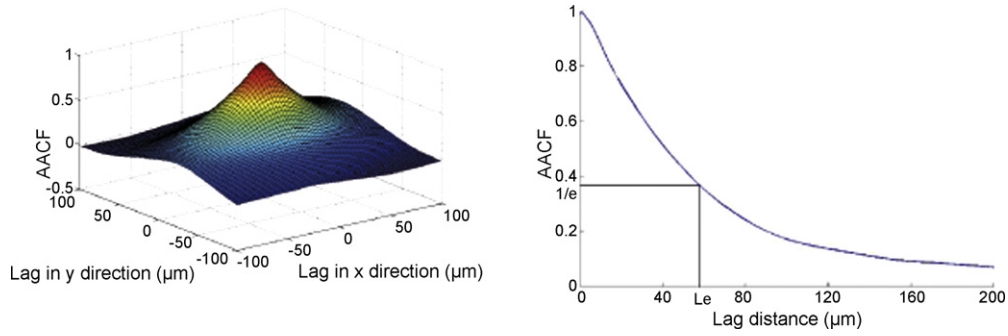


Fig. 2. L_c calculation from surface and profile mapping.

2.4. Gloss theory

Gloss relates to the ability of a surface to direct reflected light. The term gloss includes large varieties of surface phenomena constituting the light-reflecting properties of a surface. The most well known type of gloss, and the one we will focus on, is the specular gloss.

Specular reflection is defined as the ratio of the intensity of the reflected beam to the intensity of the incident beam of light at a specific angle of incidence. The angle of incidence, θ , is referenced to the surface normal.

For isotropic, homogeneous, optically smooth surfaces that do not show diffuse reflection and are essentially nonabsorbing, specular reflectance is only governed by the index of refraction, the angle of incidence of the light, and the polarization state of the incident light. For optically smooth surfaces (e.g., a mirror), the specular reflection can be calculated from Fresnel's theory (Arino et al., 2005):

$$\rho(\theta, \lambda) = \frac{1}{2} \left[\left(\frac{\cos \theta - \sqrt{n\lambda^2 - \sin^2 \theta}}{\cos \theta + \sqrt{n\lambda^2 - \sin^2 \theta}} \right)^2 + \left(\frac{n\lambda^2 \cos \theta - \sqrt{n\lambda^2 - \sin^2 \theta}}{n\lambda^2 \cos \theta + \sqrt{n\lambda^2 - \sin^2 \theta}} \right)^2 \right] \quad (4)$$

where $n(\lambda)$ is the index of refraction at the wavelength, λ .

In the case of the paper surface, the rough and anisotropic nature of the surface brings tremendous difficulties to model the specular reflectance, ρ , of the paper surface.

Chinmayanandam (1919) proposed a modelization relating the gloss of a surface to its roughness. He assumed that the surface elements responsible for the gloss were normally distributed. Hence he suggested the expression given in Eq. (5) of the scattered intensity I :

$$I = \exp \left(-\frac{8\pi^2 \cos^2 R_\theta}{\alpha\lambda^2} \right) \quad (5)$$

where R_θ is the view angle, α a constant in m^{-2} and λ the wavelength.

Improvements of Eq. (5) were made to take into account the roughness (Beckmann, 1963):

$$\frac{I}{I_0} = \rho(\theta, \lambda) \exp \left(-\frac{4\pi S_q \cos \theta}{\lambda} \right)^2 \quad (6)$$

Eq. (6) has been intensively used. However, many cases of surfaces with close values of S_q but with different values of gloss were reported (Bliznyuk et al., 2002).

Besides, one of the assumptions is that the wavelength is smaller than the roughness. However, within the visible spectrum such a

condition is achieved for only few types of paper grades (coated paper and photographic papers for instance).

Models based on surface light diffusion were also constructed, leading to a more complicated equation. For a 1D case, the scattered intensity I is expressed in Eq. (7) (Bliznyuk et al., 2002):

$$I = R^2 \int \exp[-k^2\sigma^2(1 - A\tau)] \exp \left(-\frac{jkw\tau}{f} \right) d\tau \quad (7)$$

with $A(\zeta)$ is the autocorrelation function of the surface, R the reflectance of the sample, ζ the distance between two points of the surface, w the angular frequency, k is the wave number, and f the local length of the incident radiation.

A semi-empirical model based on the Kirchoff theory for exponentially distributed surface was developed by Alexandra-Katz and Barrera (1998), who introduced a ratio $(L_c/\lambda)/(S_q/\lambda)^2$, in order to relate the topographical surface characteristic to gloss. This model was successfully applied by Caner and Farnood (2006) for micro-gloss measurement application.

All these models relate S_q or L_c to the level of gloss without giving information on the scale of measurements and the discretization step of the topographical data. However, as studies suggested, this scale may have a huge influence on the results. Indeed, a multi-scale characterization of the evolution of S_q and L_c function of the evolution of the surface due to calendering is needed.

2.5. Calendering operational conditions

The laboratory calendering machine is composed of two rolls (one metallic and one elastic) each with a 300-mm width. The metallic roll is chromed and has a diameter of 130 mm; the elastic roll coated with rubber has a diameter of 180 mm (and its hardness is Pj89ShD).

The linear load can vary from 0 kNm^{-1} to 100 kNm^{-1} (corresponding, with respect to the width of the nip, to a pressure varying between 0 bar and 40 bar). The speed of the sheet is 22.5 m min^{-1} . The temperature of the nip can be regulated from 0°C to 100°C .

We fixed four conditions of calendering (referenced respectively as "C1" to "C4").

For each of these cases, the same sheet of Q+ and Q− was calendered six times. After each pass, a given area was optically analyzed with the IFM at four different magnifications: namely 5×, 10×, 20× and 50×, respectively. The advantage of this methodology is to measure exactly the same area after each pass.

To control the homogeneity of the effect of the process, four other areas were analyzed with a 10× magnification. Hence, for each operational condition, each paper grade and after each pass in the calendering nip, five measurements under the magnification 10× were performed.

3. Experimental results

3.1. Paper surface multi-scale roughness analysis

Surface mapping is obtained from IFM measurement. The images consisted in 1024×1024 pixels (noted $L \times L$) where a pixel represents 1600 nm, 800 nm, 400 nm, 160 nm and 80 nm for the magnifications $5\times$, $10\times$, $20\times$, $50\times$ and $100\times$, respectively. Varying the magnifications of the IFM microscope induces two parameters modification: the surface evaluation size and the step of discretization. As the magnification increase, the surface evaluation size decreases while the step of discretization increases.

Fig. 3 demonstrates the relation between the S_q value of the considered papers and the magnifications chosen for the measurement of the objectives $5\times$, $10\times$, $20\times$, $50\times$ and $100\times$. The results are averaged for 20 measurements for each magnification.

As a matter of fact, the S_q value of the samples considered decreases with the increasing magnification. The analysis of the error bar of the measurements for each magnification may be related to the paper surface homogeneity at each scale considered. It appears that the dispersions (the error bar in Fig. 3 represents the standard deviation) of paper the Q– are large and are getting larger with an increasing magnification. Furthermore, these dispersions are smaller for paper Q+.

The S_q evolutions presented in Fig. 2 are plotted vs. the magnification. However, the effect of the evaluation length and the discretization is not taken into account independently.

From the surface measurements of the studied papers, the geometric average height (S_q) and the correlation length (L_c) were calculated independently as a function of both the evaluation length (defined as the length of the edge of the square where the calculation is performed) and the step of discretization.

The algorithm, developed for the multi-scale study computed the value of S_q and L_c for a given evaluation length l and a given position (x, y) for the surface referred to as i . A step of growth for the evaluation length is chosen, $\Delta = \Delta x = \Delta y = 1$ pixel. The first step is to divide the initial surface into equally sized squares having an edge of l_0 (l_0 is taken equal to $2 \mu\text{m}$). Then for each of these squares (indexed as t) local values of $S_q^t(l_0, i)$ and $L_c^t(l_0, i)$ are calculated according to the local mean plan. Then the local values are averaged to calculate $S_q(l_0, i)$ and $L_c(l_0, i)$ corresponding to the observation scale l_0 . Then new squares are extracted from the original surface i with an edge of $l_1 = l_0 + \Delta$. The operation is repeated until $l_n = L$.

The dependence on the roughness regarding the evaluation length can be integrated in the fractal concept, which aims to find invariant scale parameters. The most common method for roughness analysis is based on the Mandelbrot (1985) works. Fractal

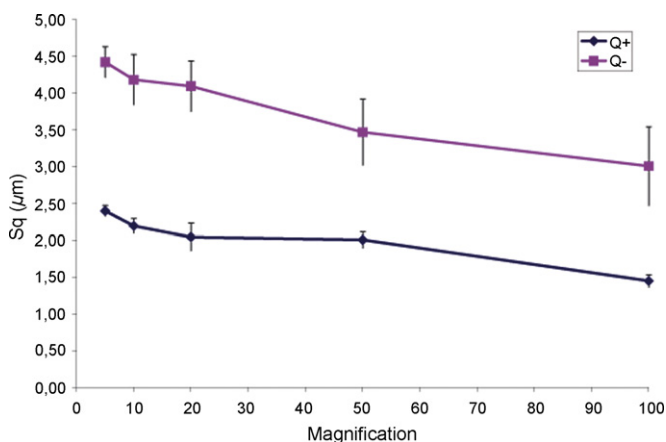


Fig. 3. S_q variation vs. magnification for the considered papers.

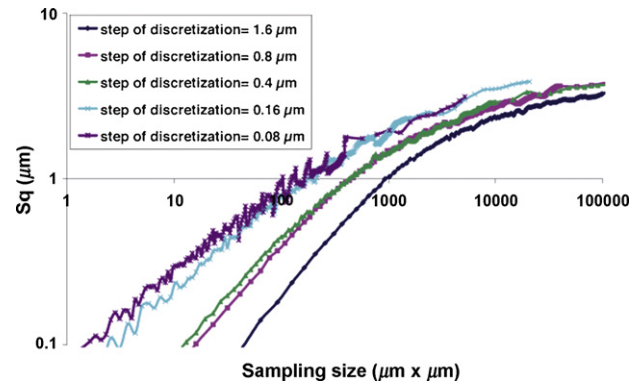


Fig. 4. S_q evolutions for the paper Q– as a function of the surface size in a log–log representation considering the step of discretization ($5\times$, $10\times$, $20\times$, $50\times$ and $100\times$, respectively) as a parameter.

surfaces own a linear relationship between roughness parameters and the length of evaluation in log–log representation. The slope of the curve $H = (\Delta \log_{10} S_q) / (\Delta \log_{10} l)$ is related to the Holder exponent which allows for the calculation of the fractal dimension F of the considered surface ($F = 2 - H$). The fractal behaviour of paper surfaces was studied using several approaches: Kent (1991) determined the fractal dimension of paper form surface topography. Chinga (2006) introduced a quadtree decomposition approach for assessing surface structures of paper.

Fig. 4 presents the S_q evolutions for the paper Q– as a function of the surface size in a log–log representation considering the step of discretization as a parameter.

The other paper (paper Q+) studied presents similar evolution.

The influence of the step of discretization is shown in this graph. As a matter of fact, for a given surface size, the S_q value of the paper is strongly dependent on this discretization. Hence the multi-scale behaviour is confirmed. Unsurprisingly, the highest roughness values are obtained for the biggest discretization steps. Therefore, this representation allows for the quantification of the relationship between the roughness value and the surface size of the sample. Furthermore all the considered curves present different stages. Basically the evolution can be divided into three linear stages in the log–log representation. Using the Mandelbrot theorem (Mandelbrot, 1985), the Holder exponent can be calculated (for the linear stage in the log–log representation) and then the fractal dimension of each different stage could be extracted. This methodology was successfully applied to the study the micro-machined surface (Bigerelle et al., 2007) and paper surface roughness (Vernhes et al., 2008a).

Fig. 5 presents the L_c evolutions for the paper Q+ as a function of the surface size in a log–log representation considering the step of discretization as a parameter.

The correlation length variation is almost linear for the whole domain of investigation (in a log–log representation). Hence, only one Holder exponent is associated to the correlation length for a given magnification. The effect of the discretization on L_c is smaller than for S_q (comparing Figs. 4 and 5). We may note that the highest values are obtained for the smaller magnification.

3.2. Evolution of roughness in function of the number of nip passes

The normalized S_q variations ($S_{q,norm} = (S_{q_o} - S_{q_n}) / S_{q_o}$ where the subscripts norm, o and n refers to normalized, initial, and after n passes, respectively). The variations of the paper according to the number of passes in the calendaring nip + with a constant pressure (40 bar) and a given temperature (20°C) and for the four chosen magnifications are presented in Fig. 6.

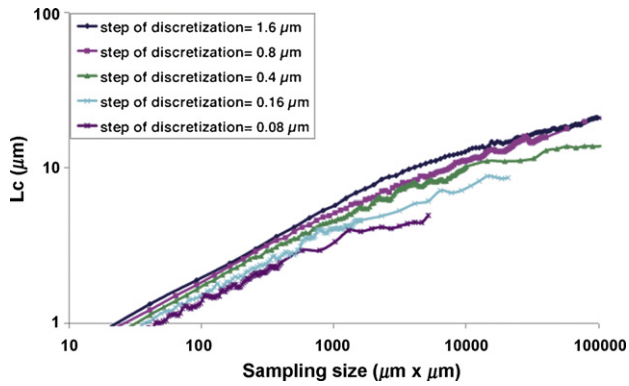


Fig. 5. L_c evolutions for the paper Q+ as a function of the surface size in a log–log representation considering the step of discretization (5 \times , 10 \times , 20 \times , 50 \times and 100 \times , respectively) as a parameter.

An interesting result occurs with the magnification at 5 \times (1 pixel = 1.6 μm). The S_q value increases with the number of passes. We assume that the calendering affects the short wavelengths of the roughness, while the undulation could be increased. As the 5 \times magnification reveals the larger wavelength, this could explain the obtained results.

For the two papers and the four experimental conditions considered, the S_q variation was maximized for the 10 \times magnification (1 pixel = 0.8 μm). We believe that the compression of the fibers and the rearrangement of the surface structure occurs in the range of size measured with the 10 \times magnification (surface size of 800 $\mu\text{m} \times 800 \mu\text{m}$). Let's remember that a typical width of a wood fiber is about 25–40 μm while its length has an order of magnitude of 1 mm.

The influences of both the processing conditions and the paper grade are exhibited in Fig. 7 under the 10 \times magnification. Both the temperature and the pressure were modified.

As a matter of fact similar shapes are obtained for all the experimental conditions; the first two passes in the calendering nip significantly decrease the value of S_q . Then the fluctuations get smaller and a stabilization is eventually reached. Moreover, the S_q variations of the paper Q– are higher than the paper Q+ which is originally smoother.

For both paper grades the same rating is obtained. The biggest variations are obtained for the highest temperature and the highest pressure. The minimum changes are obtained with the minimum pressure and the lowest temperature. Furthermore, temperature seems to have a greater influence than pressure. The S_q evolutions for both Q+ and Q– papers are higher when the temperature is fixed at 100 $^\circ\text{C}$ with 25 bar of pressure, than when the temperature is 20 $^\circ\text{C}$ with 40 bar of pressure.

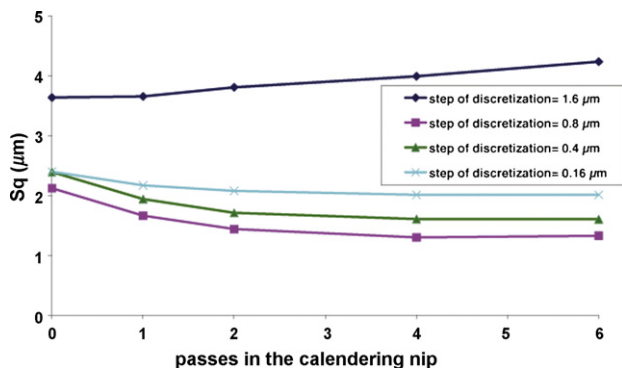


Fig. 6. Normalized variation of S_q according to the number of nips for Q+ (condition C2: linear load = 100 kN m^{-1} and $t = 20^\circ\text{C}$).

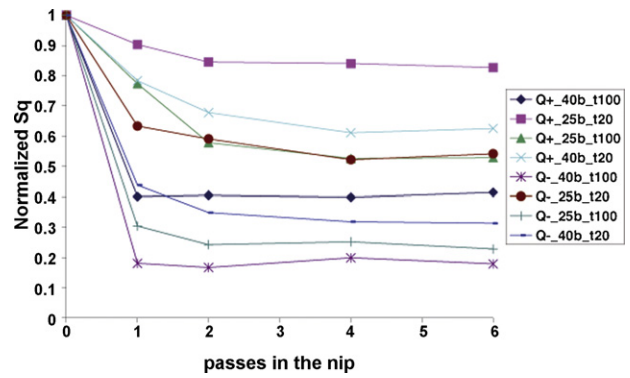


Fig. 7. Normalized variation of S_q for both papers Q+ and Q– for different conditions of pressures (25–40 bar) and temperatures (20–100 $^\circ\text{C}$) (magnification of the measurements is 10 \times).

The variations of $S_{q, \text{norm}}$ were maximized for a magnification of 10 \times . The next step is to analyse within this discretization step, the effect of the evaluation length. We applied the algorithm described in Section 3.1 to evaluate the multi-scale behaviour of S_q and L_c for a step of discretization of 0.8 μm according to the number of passes in the nip. The results are presented in Fig. 8.

The variations of the correlation length function of the number of passes in the nip strongly depend on the evaluation length. As a matter of fact, for small evaluation lengths (<200 μm), almost no calendering effects are noticeable. However, for large evaluation lengths (>800 μm), the first pass in the calendering machine implies a decrease of L_c . The next passes then do not have much further effect on L_c . The variation of the correlation length is mostly dependent on the heated temperature, as the previous observation stands for the heated series C1 and C3. For the conditions C2 and C4, the correlation length does not vary much even if a small decrease can be noticed.

Fig. 9 presents the evolution of S_q as a function of the evaluation length according to the number of passes in the nip for the paper Q– (condition C1: $p = 40$ bar and $t = 20^\circ\text{C}$).

A gap exists between the S_q value of the virgin paper and the samples which have been calendered for the whole domain of investigation. Then, the differences between the different passes is small (but exists), especially for the evaluation length inferior to 100 μm . For the larger evaluation lengths (>300 μm) the effect of the calendering is more pronounced.

When the samples are heated, the S_q variations are limited to the first pass (see Fig. 10), and then almost no variation occurred for further passes in the nip for large evaluation length.

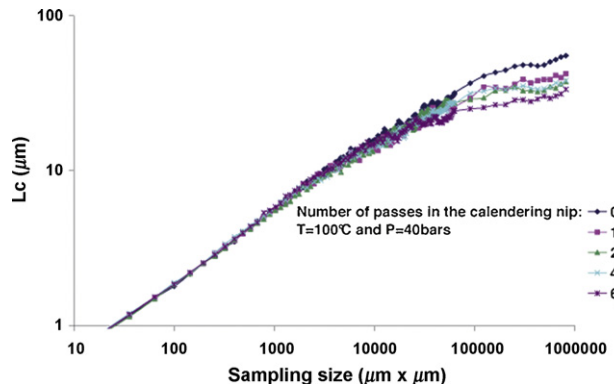


Fig. 8. Correlation length (L_c) evolution as a function of the evaluation length according to the number of passes in the nip for the paper Q+ (magnification 10 \times , condition C1: $p = 40$ bar and $t = 100^\circ\text{C}$).

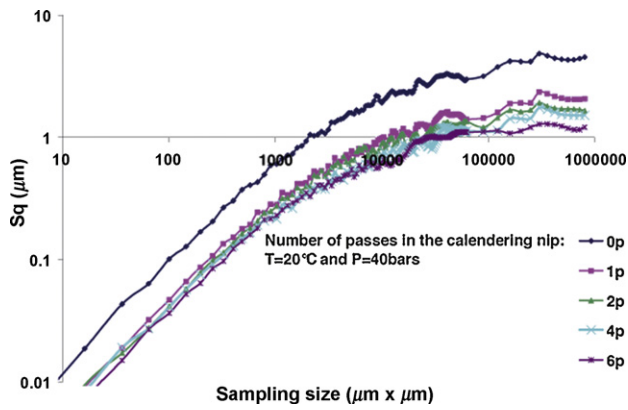


Fig. 9. Evolution of S_q as a function of the evaluation length according to the number of passes in the nip for the paper Q- (magnification 10 \times , condition C2: $p=40$ bar and $t=20^\circ\text{C}$).

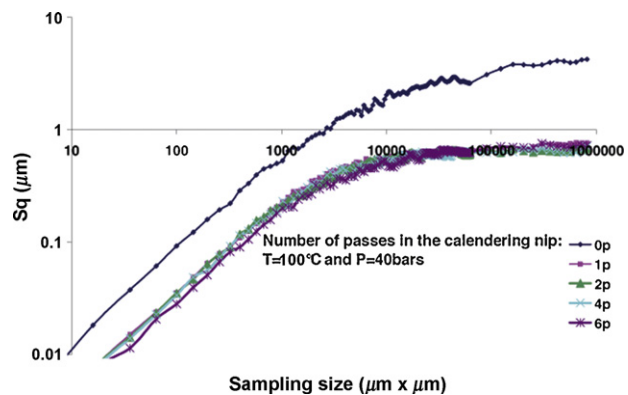


Fig. 10. Evolution of S_q as a function of the evaluation length according to the number of passes in the nip for the paper Q- (magnification 10 \times , condition C1: $p=40$ bar and $t=100^\circ\text{C}$).

However, for small evaluation lengths ($l < 100 \mu\text{m}$) the roughness respect the passes in the nip. Therefore, it seems that when the calendering involves heat transfer, the small scales of the structure are affected more than the bigger ones.

The ratio $(L_c/\lambda)/(S_q/\lambda)^2$ developed by Alexandra-Katz and Barrera (1998) relates the topographical surface characteristic to gloss by taking into account both parameters L_c and S_q . We further extend the examination of the surface topography by calculating this ratio using the multi-scale analysis (Fig. 11).

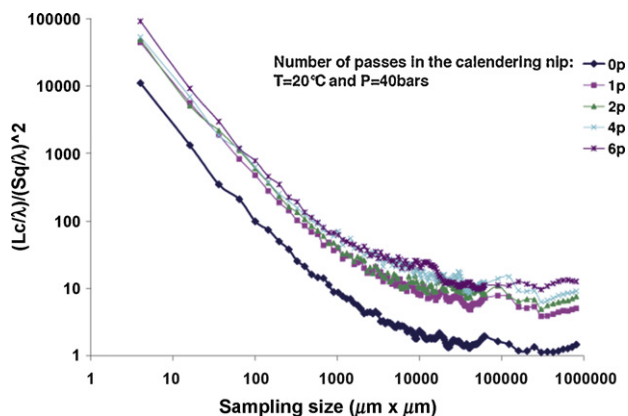


Fig. 11. Evolution of the ratio $(L_c/\lambda)/(S_q/\lambda)^2$ as a function of the evaluation length according to the number of passes in the nip for the paper Q- (magnification 10 \times , condition C2: $p=40$ bar and $t=20^\circ\text{C}$).

From Fig. 11 the quantification of the gloss can be achieved. As a matter of fact, sample with the higher value of the ratio $(L_c/\lambda)/(S_q/\lambda)^2$ will be glossier. The value of the ratio for the different states of calendering decreases with an increasing sampling size. Nevertheless, it tends to stabilize for sampling size above 10,000 μm^2 (corresponding to an evaluation length of 100 μm). Hence, from these results it is possible to define minimum surface measurements to relate topography to gloss.

4. Conclusion

The surfaces of paper surface were modified using different calendering conditions (temperature and pressure). The evolution of the main surfaces descriptors (the root mean square S_q and the correlation length L_c) function of the process condition was studied. Indeed, a new method was developed permitting the study of the dependency of these two parameters to both the evaluation length and the step of discretization. We obtained a step of discretization (0.8 μm) where the effect of the calendering on the statistical parameters was maximized. This size corresponds to 20 times the characteristic feature of the surface (the width of a single wood fiber). The effects of calendering on the correlation length were more pronounced for large evaluation length ($>200 \mu\text{m}$). The effect of the evaluation length on the root mean square (S_q) depends on the heating condition of the sample. Larger variation of S_q for the un-heated sample occurs for large evaluation length ($>300 \mu\text{m}$), while the heated samples are more affected for the small evaluation length ($<100 \mu\text{m}$). Hence, the multi-scale effect of calendering on the paper surface micro-structure was demonstrated. This multi-scale approach could therefore be incorporated into refined gloss model.

References

- Alexandra-Katz, R., Barrera, R.G., 1998. Surface correlation effect on gloss. *J. Polym. Sci., Part B: Polym. Phys.* 36, 1321–1334.
- Arino, I., Kleist, U., Mattsson, L., Rigdahl, M., 2005. On the relation between surface texture and gloss of injection-molded pigmented plastics. *Polym. Eng. Sci.* 45, 1343–1356.
- Arney, J.S., Ye, L., Wible, J., Oswald, T., 2006. Analysis of paper gloss. *J. Pulp Pap. Sci.* 32, 19–23.
- Beckmann, P.S.A., 1963. *The Scattering of Electromagnetic Waves from Rough Surfaces*. Pergamon Press, London.
- Beland, M.C., Bennet, J., 2000. Effect of local microroughness on the gloss uniformity of printed paper surfaces. *Appl. Opt.* 39, 2719–2726.
- Bigerelle, M., Gautier, A., Iost, A., 2007. Roughness characteristic length scales of micro-machined surfaces: a multi-scale modelling. *Sens. Actuators B* 126, 126–137.
- Bliznyuk, V., Assender, H., Porfyakis, K., 2002. How surface topography relates to material's properties. *Mater. Sci. Eng. B* 297, 973–976.
- Bloch, J.F., Rolland du Roscoat, S., Mercier, C., Vernhes, P., Pineaux, B., Blayo, A., Mangin, P., 2006. Influence of paper structure on printability: characterisation using X-ray synchrotron microtomography. *NIP Denver*, 449–453.
- Caner, E., Farnood, R., 2006. Effect of the coating formulation on the gloss properties of coated papers. In: *International Printing and Graphic Arts Conference*, Miami, pp. 1–18.
- Chinga, G., 2004. Detailed characterization of paper surface structure for gloss assessment. *J. Pulp Pap. Sci.* 30, 222–227.
- Chinga, G., 2006. A quadtree decomposition approach for surface assessment. *Pattern Anal. Appl.* 9, 94–101.
- Chinga, G., Helle, T., 2002. Structure characterisation of pigment coating layer on paper by scanning electron microscopy and image analysis. *Nord. Pulp Pap. Res. J.* 17, 307–312.
- Chinmayanandam, T.K., 1919. On the specular reflection from rough surfaces. *Phys. Rev.* 13, 96.
- Gate, L., Windle, W., Hine, M., 1973. The relationship between gloss and surface microstructure of coatings. *Tappi J.* 56, 61–65.
- Hamel, J., Dostie, M., 1997. Convective heat transfer in calendering. *J. Pulp Pap. Sci.* 23, 77–85.
- Holmstad, R., Kure, K.A., Chinga, G., Gregersen, O.W., 2004. Effect of temperature gradient multi-nip calendering on the structure of SC paper. *Nord. Pulp Pap. Res. J.* 19, 489–494.
- ISO 25178-6. Geometrical product specifications (GPS)—Surface texture: Areal—Part 6: Classification of methods for measuring surface texture, 2007.

- Kent, H., 1991. The fractal dimension of paper surface topography. *Nord. Pulp Pap. Res. J.*, 191–196.
- Lepoutre, P., Means, G., 1978. Supercalendering and coating properties. *Tappi J.* 61, 85–87.
- Lettieri, T.R., Marx, E., Song, J., Vorburger, T.V., 1993. Light scattering from glossy coatings on paper. *Appl. Opt.* 30, 4439–4447.
- Litvinov, V., Farnood, R., 2006. Modeling thickness and roughness reduction of paper in calendering. *Nord. Pulp Pap. Res. J.* 21, 365–371.
- Mandelbrot, B., 1985. Self-affine fractals and fractal dimension. *Phys. Scripta* 32, 257–260.
- Patrikar, R.M., 2004. Modeling and simulation of surface roughness. *Appl. Surf. Sci.* 228, 213–220.
- Roscoat, S.R.D., Decain, M., Geindreau, C., Thibault, X., Bloch, J.F., 2007. Microstructural analysis of paper using synchrotron X-ray microtomography: numerical estimation of the permeability and effective thermal conductivity. *Appita* 61, 286–301.
- Stout, K.J., 2000. *Development of Methods for the Characterisation of Roughness in Three Dimensions*. Penton Press, London.
- Suontausta, O., 2002. Coating and calendering—means of improving surface of coated paper for printing. Ph.D. Thesis, Helsinki University of Technology, Espoo.
- Vernhes, P., Bloch, J.F., Blayo, A., Mercier, C., Pineaux, B., 2008a. Statistical analysis of paper surface microstructure: a multi-scale approach. *Appl. Surf. Sci.* 254, 7431–7437.
- Vernhes, P., Rolland du Roscoat, C.-S., Blayo, A., Pineaux, B., Bloch, J.F., 2008b. Synchrotron X-ray microtomography: a new tool to characterize the interaction between paper and toner. *J. Imaging Sci. Technol.* 52, 6.
- Wu, J.-J., 2000. Characterization of fractal surfaces. *Wear* 239, 36–47.